The Role of Driving Energy and Delocalized States for Charge Separation in Organic Semiconductors

Artem A. Bakulin, *et al.*

Science **335**, 1340 (2012);
DOI: 10.1126/science.1217745

states is favored over the ground-state channel. Once again, this agrees well with the experimental mass spectrum and CRATI results for *n*-butane (Fig. 2). These theoretical results show that direct ionization into multiple ionic states can be understood as a subcycle phenomenon. Qualitatively, the SFI response of these two molecules can be understood by considering the ionization energies and Dyson orbitals given in table S4. The Dyson orbitals represent the initial single-particle state of the ionizing electron. Within the Hartree-Fock approximation and Koopmans picture, they become ionization channels from the HOMO, HOMO–1, HOMO–2, etc. In a tunneling picture, SFI depends exponentially on the I_P through the Keldysh factor $\exp[-(2/3)(2I_P)^{3/2}/E_0]$. Furthermore, for diatomics (*37*) it is known that nodal planes in the Dyson orbitals can cause strong suppression of the total yield of SFI. For the case of 1,3-butadiene, although the 1^2A_u excited state has fewer nodal planes than the 1^2B_g ground state, the large energy gap favors the ground state. For the case of *n*-butane, where the energy gaps are much smaller, orbital symmetry effects become more pronounced. The Dyson orbitals for *n*-butane reveal that the 2^2A_g excited state has the fewest nodal planes; hence, this state experiences the least suppression, rendering it the dominant SFI channel as seen in Fig. 3A.

An important question is the role of laser-driven nonadiabatic interchannel coupling (also known as NME) in polyatomics. As discussed in the SOM, the hydrocarbons irradiated here at a peak intensity of ~10^{13} W/cm^2 (798 nm) exhibited predominantly adiabatic multichannel SFI dynamics. However, at higher intensities, the role of NME in even simple diatomics remains under active debate (*6*, *15*). With our TDSE method, we can artificially turn off the laser-driven interchannel coupling in the theory and compare the result to the case where the coupling is retained. This procedure accentuates the effects of NME on the ionic-state population distribution during SFI. In Fig. 3B, we present theoretical channel-resolved SFI yields in *n*-butane using a half-cycle pulse of higher intensity (1.5×10^{14} W/cm^2, 800 nm), both with (purple) and without (blue) NME coupling. For simplicity, only the ^2A_g ground state and the ^2B_u excited state were included, as these are the continuum channels most strongly dipole-coupled by the field. As seen in Fig. 3B, along two molecular frame directions *x* (middle) and *y* (right), coherent subcycle redistribution of population between electronic continuum channels occurs when NME is included. This qualitatively demonstrates that, at intensities typical of HHG experiments, the nonadiabatic population of multiple electronic continua can be another important contributor to the attosecond molecular response.

Although the present study does not address the tacit coherences created between ionic states (*2*), the CRATI method directly reveals the population of multiple electronic continua in the SFI of polyatomic molecules. A future extension of this method that measures fragment ion energy and/or angular distributions will be of interest. Studying CRATI spectra as a function of molecular electronic structure, molecular frame alignment, and laser frequency/intensity will illuminate the role of multiple electronic continua in attosecond SFI spectroscopies such as HHG.

References and Notes

1. F. Krausz, M. Yu. Ivanov, *Rev. Mod. Phys.* **81**, 163 (2009).
2. E. Goulielmakis *et al.*, *Nature* **466**, 739 (2010).
3. G. Sansone *et al.*, *Nature* **465**, 763 (2010).
4. M. Uiberacker *et al.*, *Nature* **446**, 627 (2007).
5. O. Smirnova *et al.*, *Nature* **460**, 972 (2009).
6. S. Haessler *et al.*, *Nat. Phys.* **6**, 200 (2010).
7. H. J. Wörner, J. B. Bertrand, D. V. Kartashov, P. B. Corkum, D. M. Villeneuve, *Nature* **466**, 604 (2010).
8. J. Itatani *et al.*, *Nature* **432**, 867 (2004).
9. C. Vozzi *et al.*, *Appl. Phys. Lett.* **97**, 241103 (2010).
10. Y. Huismans *et al.*, *Science* **331**, 61 (2011).
11. M. Meckel *et al.*, *Science* **320**, 1478 (2008).
12. P. B. Corkum, *Phys. Rev. Lett.* **71**, 1994 (1993).
13. X.-B. Zhou *et al.*, *Phys. Rev. Lett.* **102**, 073902 (2009).
14. H. Akagi *et al.*, *Science* **325**, 1364 (2009).
15. S. Petretti, Y. V. Vanne, A. Saenz, A. Castro, P. Decleva, *Phys. Rev. Lett.* **104**, 223001 (2010).
16. M. Lezius *et al.*, *Phys. Rev. Lett.* **86**, 51 (2001).
17. M. Smits, C. A. de Lange, A. Stolow, D. M. Rayner, *Phys. Rev. Lett.* **93**, 203402 (2004).
18. A. N. Markevitch *et al.*, *Phys. Rev. A* **68**, 011402 (2003).
19. Z. B. Walters, S. Tonzani, C. H. Greene, *J. Phys. Chem. A* **112**, 9439 (2008).
20. D. J. Fraser *et al.*, *J. Phys. B* **28**, L739 (1995).
21. P. Agostini, F. Fabre, G. Mainfray, G. Petite, N. Rahman, *Phys. Rev. Lett.* **42**, 1127 (1979).
22. K. J. Schafer, B. Yang, L. F. DiMauro, K. C. Kulander, *Phys. Rev. Lett.* **70**, 1599 (1993).
23. C. I. Blaga *et al.*, *Nat. Phys.* **5**, 335 (2009).
24. H. Rottke, J. Ludwig, W. Sandner, *J. Phys. At. Mol. Opt. Phys.* **29**, 1479 (1996).
25. X. Zhou *et al.*, *Phys. Rev. Lett.* **100**, 073902 (2008).
26. B. K. McFarland, J. P. Farrell, P. H. Bucksbaum, M. Gühr, *Science* **322**, 1232 (2008).
27. I. Thomann *et al.*, *J. Phys. Chem. A* **112**, 9382 (2008).
28. W. Li *et al.*, *Science* **322**, 1207 (2008).
29. P. B. Armentrout, T. Baer, *J. Phys. Chem.* **100**, 12866 (1996).
30. W. A. Chupka, in *Chemical Spectroscopy and Photochemistry in the VUV*, C. Sandorfy, P. Ausloos, M. B. Robin, Eds. (North Atlantic Treaty Organization Advanced Study Institute Series, Reidel, Dordrecht, 1974), pp. 433–464.
31. R. Bombach, J. Dannacher, J.-P. Stadelmann, *J. Am. Chem. Soc.* **105**, 1824 (1983).
32. J. Dannacher, J.-P. Flamme, J.-P. Stadelmann, J. Vogt, *Chem. Phys.* **51**, 189 (1980).
33. W. A. Chupka, J. Berkowitz, *J. Chem. Phys.* **47**, 2921 (1967).
34. L. J. Frasinski *et al.*, *Phys. Rev. A* **46**, R6789 (1992).
35. R. R. Freeman *et al.*, *Phys. Rev. Lett.* **59**, 1092 (1987).
36. M. Spanner, S. Patchkovskii, *Phys. Rev. A* **80**, 063411 (2009).
37. J. Muth-Böhm, A. Becker, F. H. M. Faisal, *Phys. Rev. Lett.* **85**, 2280 (2000).
38. G. Bieri, F. Burger, E. Heilbronner, J. P. Maier, *Chim. Acta* **60**, 2213 (1977).
39. D. M. P. Holland *et al.*, *J. Phys. At. Mol. Opt. Phys.* **29**, 3091 (1996).

Acknowledgments: We thank the Natural Sciences and Engineering Research Council of Canada for financial support and R. Lausten, B. J. Sussman, D. J. Moffatt, and D. Guay for expert assistance. J.M. thanks the Feodor Lynen program of the Alexander von Humboldt Foundation for financial support. Aspects of this work are part of the research program of the Stichting voor Fundamenteel Onderzoek der Materie (FOM), which is financially supported by the Nederlandse Organisatie voor Wetenschappelijk Onderzoek (NWO). The authors declare no competing financial interests.

Supporting Online Material

www.sciencemag.org/cgi/content/full/335/6074/1336/DC1
Methods
SOM Text
Figs. S1 to S6
Tables S1 to S4
References (*40*–*45*)

19 August 2011; accepted 21 January 2012
10.1126/science.1212896

The Role of Driving Energy and Delocalized States for Charge Separation in Organic Semiconductors

Artem A. Bakulin,[1]* Akshay Rao,[1] Vlad G. Pavelyev,[2] Paul H. M. van Loosdrecht,[2] Maxim S. Pshenichnikov,[2] Dorota Niedzialek,[3] Jérôme Cornil,[3] David Beljonne,[3] Richard H. Friend[1]†

The electron-hole pair created via photon absorption in organic photoconversion systems must overcome the Coulomb attraction to achieve long-range charge separation. We show that this process is facilitated through the formation of excited, delocalized band states. In our experiments on organic photovoltaic cells, these states were accessed for a short time (<1 picosecond) via infrared (IR) optical excitation of electron-hole pairs bound at the heterojunction. Atomistic modeling showed that the IR photons promote bound charge pairs to delocalized band states, similar to those formed just after singlet exciton dissociation, which indicates that such states act as the gateway for charge separation. Our results suggest that charge separation in efficient organic photoconversion systems occurs through hot-state charge delocalization rather than energy-gradient–driven intermolecular hopping.

In contrast to the elegant photosynthetic apparatus evolved by nature (*1*), organic photovoltaic (OPV) cells use a single heterojunction between two semiconductors to generate charge (*2*). These semiconductors, referred to as the donor (D) and acceptor (A), are cast from solution or vacuum sublimed to form a thin film with nanoscale domains of relatively pure "bulk" materials and large interfacial regions. This architecture, known as the bulk heterojunction (*3*),

allows for absorption of light in the bulk domains to form excitons followed by charge generation at the interface where offsets between the lowest unoccupied molecular orbitals (LUMOs) and highest occupied molecular orbitals (HOMOs) of the D and A enable electron transfer, thereby dissociating the exciton.

The various conjugated macromolecules used in this study are shown in Fig. 1, along with their reported external quantum efficiencies (EQEs), under short-circuit conditions, which vary from high (>70%) to low (<10%) (*4*–*9*). This variation in performance cannot be explained simply by energy-level offsets, as these are sufficient in all listed systems to enable exciton dissociation, nor can they be explained by nonideal charge transport (*10*, *11*). Instead, fundamental differences in electronic structure of the heterojunctions formed between materials affect the efficiency of photoconversion.

The current understanding of the photon-to-charge conversion in OPV devices is illustrated in Fig. 2, A to C (*12*). Absorption of a photon produces an intramolecular singlet exciton at the D-A interface either directly or after exciton diffusion from the bulk domains. The exciton then undergoes ultrafast quasi-adiabatic charge transfer, yielding the hole on D and electron on A. Having overcome the intramolecular Coulomb attraction (holding together the singlet exciton), via the use of offset energy levels, the charges remain electrostatically attracted across the D-A interface (*10*, *13*). Because of the interaction, the nature of the state produced may differ from that of a free well-separated electron-hole pair (separated charges, SC), so hereafter we refer to the species formed immediately after charge transfer as "charge-transfer" (CT) states, without consideration of whether these states eventually dissociate into free carriers or stay bound until recombination (*14*). When electron and hole do localize, so that they are immediately adjacent on either side on the heterojunction, Coulombic binding energies of several hundred meV are expected and observed (*15*, *16*). In photosynthesis, separation of charges is achieved with the aid of cascaded energy levels and ion screening (*1*, *17*). OPVs, by contrast, possess none of these elements, yet surprisingly, some OPV systems work very efficiently (Fig. 1). Hence, the fundamental question of how the organic heterojunction enables efficient long-range charge separation remains unanswered.

Here, we address this issue by applying an electro-optical pump-push experiment, performed on working OPV diodes (Fig. 2D). A visible "pump" pulse illuminates the OPV and creates a population of CT and SC states, as illustrated in Fig. 2, A and C. The pump flux is kept low to give excitation densities ~10^{16} cm^{-3}, comparable to continuous solar excitation (*18*). The charge carrier on the polymer causes a geometrical rearrangement of the chain, known as polaron formation. Polaron formation lowers the energy for charge storage by pulling two band states (π and π^*) into the gap, creating the localized polaron illustrated in Fig. 2B (*19*, *20*). For the hole polaron, the lower gap state is singly occupied, and the optical transition (P1) between it and the π valence band is strongly allowed, forming an absorption band typically between 0.1 and 0.5 eV (*20*, *21*), with the energy being determined by the degree of polaron delocalization (*22*). As we show below, polaron formation plays a key role in limiting long-range charge separation. In

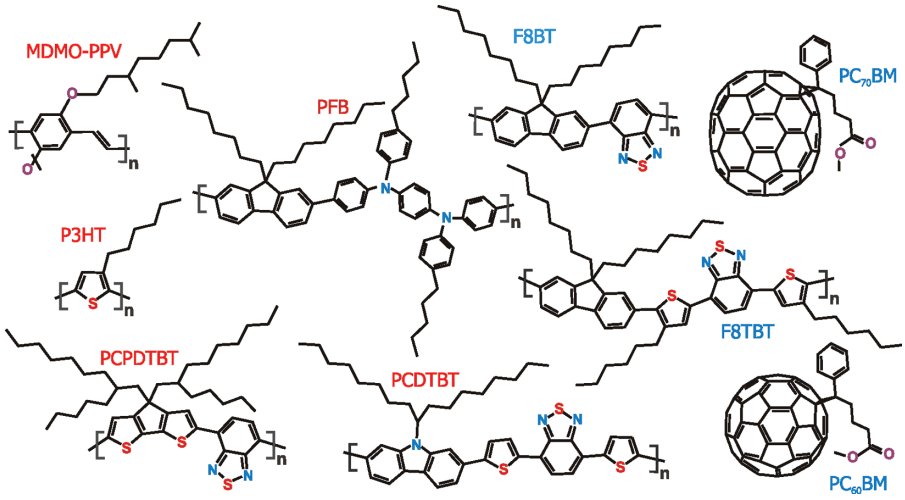

Fig. 1. Chemical structures of donor (left, red captions) and acceptor (right, blue captions) materials used in this study. Typical external quantum efficiencies of the corresponding OPVs (*4*–*9*), defined as the number of collected electrons collected per incident photon, are as follows: PFB:F8BT (6%), P3HT:F8TBT (25%), MDMO-PPV:$PC_{70}BM$ (40%), PCPDTBT:$PC_{70}BM$ (50%), P3HT:$PC_{60}BM$ (70%), and PCDTBT:$PC_{70}BM$ (80%).

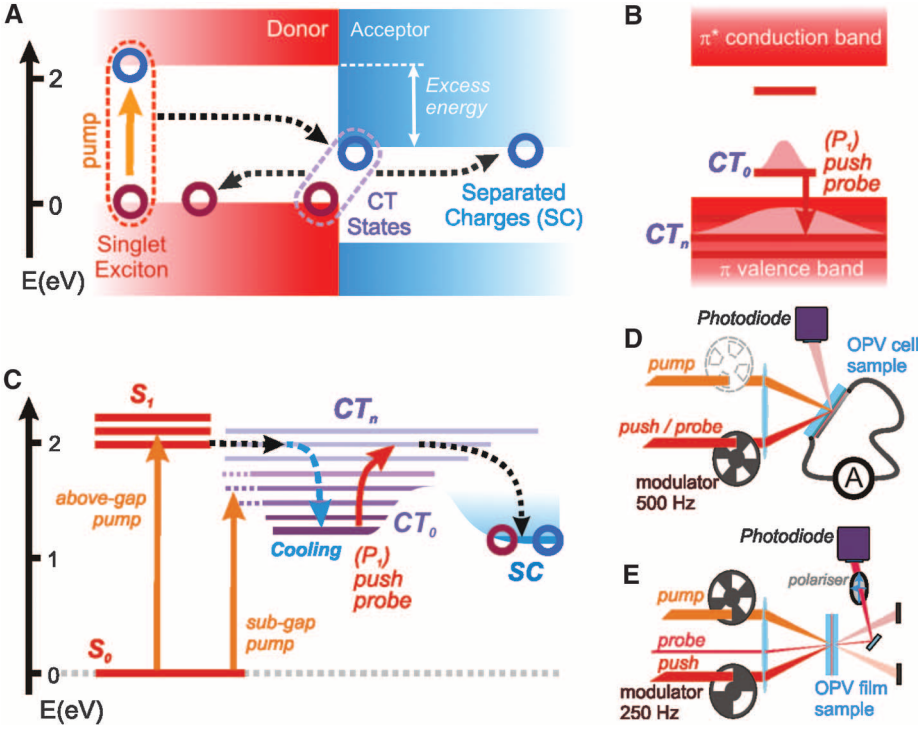

Fig. 2. (**A** and **B**) Band diagrams for (A) a typical OPV and (B) a cationic state on the polymer donor. (**C**) Free-energy state diagram of the same OPV system. Singlet, charge-transfer (CT; lowest-lying, CT_0; band states, CT_n) and separated-charges (SC) states are shown; positive charge density distribution in (B) is indicated by pink contour. Solid arrows show optical transitions, and dashed arrows indicate energy- and charge-transfer pathways involved in photoconversion. Layouts of (**D**) pump-push photocurrent and (**E**) three-pulse transient-anisotropy experiment.

[1]Cavendish laboratory, University of Cambridge, JJ Thomson Avenue, Cambridge CB30HE, UK. [2]Zernike Institute for Advanced Materials, University of Groningen, Nijenborgh 4, 9747 AG Groningen, Netherlands. [3]Laboratory for Chemistry of Novel Materials, University of Mons, Place du Parc 20, B-7000 Mons, Belgium.

*Present address: AMOLF, Science Park 104, 1098 XG Amsterdam, Netherlands.

†To whom correspondence should be addressed. E-mail: rhf10@cam.ac.uk

our experiments, we address the dynamics of electron-hole pairs still localized at the interface. After charge transfer, the CT_n states formed are "hot" states with energies of 0.3 to 1 eV in excess of the lowest-lying CT_0 states. The charge pair then relaxes through the manifold to the lowest-lying CT_0 states, giving rise to a red-shifted CT emission (*23*). Here we selectively excited the P1 (CT_0 to CT_n) transition with an infrared (IR) "push" pulse, repopulating hot states that the system samples immediately after the charge transfer. The perturbation of the charge dynamics on the molecular level affected the OPV performance, and the corresponding change of the photocurrent (δPC) induced by the IR push pulse is recorded as a function of the delay between pump and push (*24*, *25*). In a complementary all-optical experiment (Fig. 2E), the effect of the push pulse

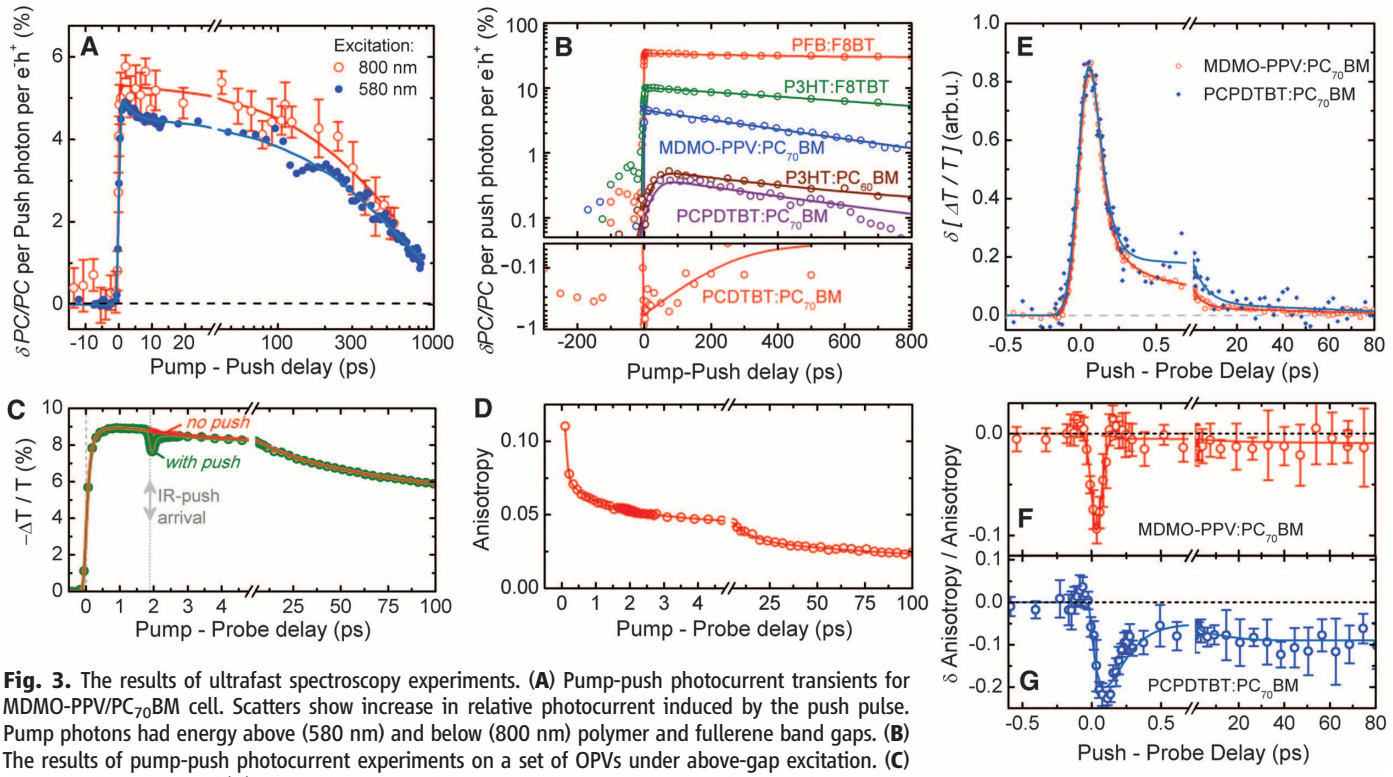

Fig. 3. The results of ultrafast spectroscopy experiments. (**A**) Pump-push photocurrent transients for MDMO-PPV/$PC_{70}BM$ cell. Scatters show increase in relative photocurrent induced by the push pulse. Pump photons had energy above (580 nm) and below (800 nm) polymer and fullerene band gaps. (**B**) The results of pump-push photocurrent experiments on a set of OPVs under above-gap excitation. (**C**) Transient-absorption and (**D**) transient-anisotropy kinetics for MDMO-PPV:$PC_{70}BM$ film excited at 580 nm and probed at 3 μm. Green line in (C) shows dynamics with push pulse arriving at ~2 ps delay. The effect of push pulse on the isotropic (**E**) and anisotropic (**F** and **G**) transients, calculated from the difference between with-push and no-push measurements, for MDMO-PPV/$PC_{70}BM$, PCPDTBT/$PC_{70}BM$ films. In all figures, solid lines are (multi)exponential fits convoluted with the Gaussian function at zero delay.

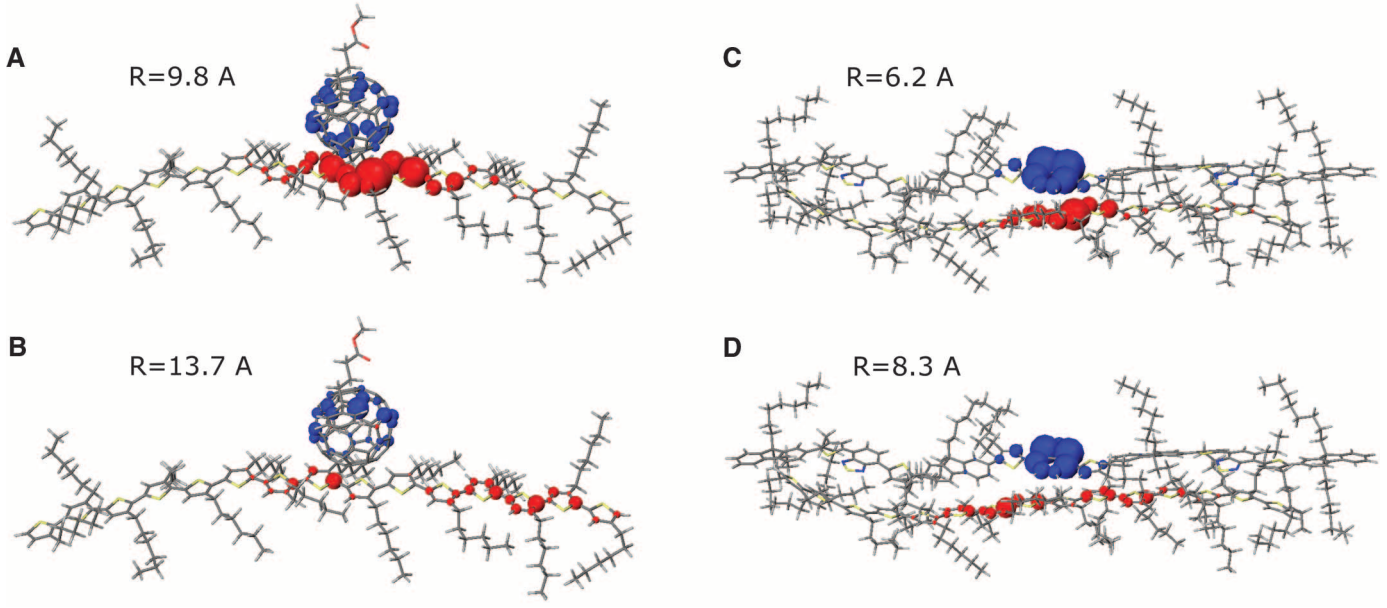

Fig. 4. Microelectrostatic simulations of the charge distribution at the P3HT/PCBM (**A** and **B**) and P3HT/F8TBT (**C** and **D**) heterojunction, with electron and hole densities shown in blue and red, respectively. (A and C) Charge distribution in the lowest CT-state configuration, and (B and D) in the excited CT-state configuration created upon absorption of an IR-push photon. R, average electron-hole separation.

on charge dynamics is observed with an additional IR "probe" pulse (*26*). To boost the signal and ensure that a large number of charges were excited by the push pulse, we used a higher excitation density (~10^{19} cm^{-3}) in the all-optical experiment.

The push-induced states were similar to those populated directly after exciton dissociation. The geometry of the polymer was different in the case of the push experiment because the chain had relaxed to form a polaronic state. However, as established earlier (*19*), the presence of the polaron distortion leaves all of the other π band states unchanged, as is also confirmed by the calculation presented in fig. S3 (*27*). This allowed us to generalize the results of our experiments to photoconverstion under solar-illumination conditions.

Figure 3A shows pump-push photocurrent data for an MDMO-PPV/$PC_{70}BM$ solar cell. When the push pulse arrived after the pump, the photocurrent manifestly increased. The rise time of this increase was instrument-limited (200 fs), indicating that the push interacted with species created directly after excitation. The magnitude of the push-induced photocurrent decayed slowly (~600 ps) as the delay time increased. We attribute this decay to the CT-state lifetime, in agreement with previous time-resolved photoluminescence measurements (*28*, *29*). From measurements of the pump-induced absorption at the push wavelength and the flux of the push pulse, we calculated the increase in the photocurrent per IR photon absorbed per charge pair. For an MDMO-PPV/$PC_{70}BM$ cell, we observed a ~5% change in relative photocurrent i.e., every IR photon absorbed by an electron-hole pair had a 5% chance of helping to dissociate it. The fast rise time (200 fs) ruled out charge trapping after diffusion to possible defect sites. We observed a longer rise of the signal for blends of P3HT and PCPDTBT, which was probably associated with delayed formation of bound states preceded by the exciton diffusion.

An important question with regard to charge separation is the role of "excess energy" that the hot CT_n state inherited from the exciton. It has been argued that this energy, which is lost during relaxation to the "cold" CT_0 state, facilitates long-range charge separation (*11*, *30*). However, this interpretation has been questioned (*31*), and the role of excess energy remains ambiguous (*14*, *32*–*35*). We elucidated the effect of excess energy on charge separation by using below-gap excitation (Fig. 3A, open circles) (*31*, *36*). Through the below-gap transition, CT states were populated directly at the D-A interface, rather than through singlet exciton dissociation. Although the cross-section of the $S_0 \rightarrow CT$ transition was low, it allowed for charge generation while bypassing the hot CT state. We note that this excitation was not necessarily to the cold CT state, but occurs with ground-state D and A geometries. Subsequent geometrical relaxation formed polaron states, giving Stokes-shifted (~0.6 eV) CT luminance (*37*). Although the CT state excited had ~0.5 eV less "excess energy" than the state created after exciton dissociation, δPC/PC kinetics (Fig. 3A) were similar for sub- and above-gap excitations, demonstrating that charge separation effectively occurred without the need for the large excess energy associated with the exciton (*31*).

Figure 3B shows pump-push transients corresponding to above-gap excitation for a range of materials systems. The relative amount of additional photocurrent stimulated by re-excitation was very dependent on the particular material. Polymer-polymer blends, PFB/F8BT and P3HT/F8TBT, displayed a large push-induced increase of photocurrent (10 to 50%). Consistent with previous reports, the CT-state lifetime in these materials was up to a few tens of nanoseconds (*38*). Polymer-fullerene cells demonstrated a modest photocurrent increase (<6%) and subnanosecond CT-state lifetimes. Finally, the highly efficient PCDTBT/$PC_{70}BM$ system showed a minor decrease in photocurrent upon IR irradiation, possibly the result of bimolecular effects.

Both free hole polarons (SC) and those bound within CT states may absorb the IR push pulse. Although recent studies have indicated that the photoinduced absorption at 0.5 eV is related to CT states (*39*, *40*), IR push photons can be also absorbed by weakly bound charges, which would contribute to the PC even without the application of the push pulse. Thus, systems with lower EQE, where the amount of bound charges is high, demonstrate greater δPC/PC response. By contrast, in the efficient photoconversion systems, where the number of CT states is reduced, the push-induced photocurrent is low. After normalization on the estimated amount of bound charges, we found that for all materials, the efficiency of charge separation from the CT state after the push was lower (roughly 50%) but still comparable to the efficiency of charge separation after the original pump pulse. This result indicates that the push pulse took those excitations that had relaxed to bound CT states back to states similar to the early-time hot states formed after the singlet exciton dissociation, giving them a second chance to dissociate.

To monitor the effect of the push pulse on the charges directly, we used an all-optical pump-push-probe technique (Fig. 2E). Figure 4A shows isotropic pump-probe transients in a MDMO-PPV/$PC_{70}BM$ film with and without the push pulse. Pump pulses created CT and SC states in the OPV material, and their evolution was monitored with the IR probe pulse. When the probe arrived after the pump, it was partly absorbed by the pump-generated carriers. The red curve in Fig. 3C reflects the population of all charged (CT_0 and SC) states as a function of time. The green circles present analogous dynamics when a push pulse, ~2 ps after the pump, brought a substantial fraction (~10%) of the charges back to the hot state CT_n (Fig. 2, B and C). This re-excitation was observed as a sudden drop in signal amplitude because fewer charges were available to absorb the probe beam. The signal then rejoined the red curve as the CT_n states relaxed to CT_0. Figure 3E presents the difference in response with and without the push pulse, for MDMO-PPV and PCPDTBT mixed with $PC_{70}BM$. A fast sub–100 fs component accounted for ~80% of the signal decay, with the residual relaxation of ~20% of states occurring on a longer but still relatively fast 1- to 20-ps time scale.

Figure 3D presents the anisotropic component of the same pump-probe transient in an MDMO-PPV/$PC_{70}BM$ film. The initial anisotropy was lower than the 0.4 limit for random distribution of dipoles, indicating that there may be (excitonic) dynamics occurring before charge generation and/or below our ~70-fs time resolution (*34*). However, the nonzero anisotropy observed indicates that the P1 transition dipole of charges partly inherited polarization memory from the singlet excitons. As charges moved from the chain on which they were created to another chain, the transition dipole moment associated with the charge acquired a different orientation, which was observed as depolarization (*34*).

Figure 3, F and G, shows the relative difference between "with-push" and "no-push" anisotropic transients. As a general trend, we observed that anisotropy was reduced by the push. The anisotropy within the pulse-overlap region dropped, probably because of the different orientation of the P1 transition dipoles in the excited state. Anisotropy dynamics at longer (>0.2 ps) delays displayed biphasic behavior. Anisotropy was lost after the push and decreased further in the following 10 to 50 ps. The loss in anisotropy after the push corresponded to the re-excited hot CT state relocalizing to the neighboring CT/SC state with a different orientation of charge-associated dipole (*13*). The continued loss of anisotropy provides further evidence that charges became more mobile after the push pulse.

The fast charge relaxation and relocalization observed in three-pulse experiments are not consistent with the currently dominant models of charge separation through relaxation-assisted intermolecular hopping. However, the observed results can be explained by hole delocalization achieved via band states. These states are formed after singlet exciton dissociation, before polaron formation occurs. Here we repopulate these states through the optically allowed IR transition. The absorption of the IR photon promotes an electron from the delocalized valence band to the localized HOMO, instantaneously delocalizing the hole, as illustrated schematically in Fig. 2B. Such delocalization would then play a critical role in overriding the Coulomb binding energy (*41*).

To confirm this hypothesis, we resorted to atomistic "many-body" modeling. We first demonstrated that optical excitation from the singly (positively) charged ground state to the lowest dipole-allowed electronic state, namely, the $CT_0 \rightarrow CT_n$ (P1) electronic transition in the simplified one-electron picture above, resulted in an increased intrachain hole delocalization in isolated chains of archetypal conjugated polymers (*27*). By combining force-field geometry optimization with

quantum-chemical excited-state calculations of D-A pairs, we then inferred the nature of the electronic states at representative polymer-PCBM and polymer-polymer heterojunctions. Figure 4A features the charge density distribution as calculated in the lowest charge-transfer electronic excited state (CT_0) of a P3HT/PCBM heterojunction, and Fig. 4B shows the analogous situation for a higher-lying, strongly dipole coupled to CT_0, excited state, CT_n, prepared by absorption of an IR photon from CT_0. The P3HT-hole wave function, which was confined close to the PCBM electron in the CT_0 state, was more delocalized along the polymer backbone in the CT_n state, resulting in an increased average intermolecular electron-hole separation. The electron density on the fullerene was also changed upon the excitation to the CT_n state; however, as the electron is already delocalized on the fullerene molecule, this effect is not very pronounced. Nonetheless, current calculations cannot exclude further delocalization over more than one fullerene molecule when such molecules are available. Similar results were obtained for the P3HT/F8TBT interface (Fig. 4, C and D). Thus, at both heterojunctions, the strong IR transition from the CT_0 to the CT_n excited state, which correlates with the valence → n transition in a single P3HT chain, delocalizes the hole wave function along the donor chain and thereby promotes a larger intermolecular electron-hole separation. Although this transient delocalization is short-lived (subpicosecond), as measured by the all-optical technique in Fig. 4, B and D, it allows for charges to decouple and move apart at longer time scales (10 to 50 ps).

Although the general trend of delocalization of charge by optical excitation is observed for both modeled systems, the extent of delocalization is material dependent. Moving from F8TBT to PCBM increases the average electron-hole separation by 50%. This, in turn, induces even larger variations in CT-state binding energy and dissociation probability. The results of these variations are clearly seen in Figs. 1 and 3B. This difference in delocalization of charges causes OPV systems to demonstrate markedly different quantum efficiencies.

We propose that the driving energy for charge separation in organic photoconversion systems is the energy needed to reach delocalized band states, which are critical for long-range charge separation. Although the delocalized states are extremely short-lived (<1 ps), they enable charges to override the otherwise dominant Coulomb interaction. By contrast, large band offsets are not crucial for free-charge formation. Our results provide a new framework to understand charge generation in organic systems and outline the basis for the design of improved OPVs. In particular, those materials that support delocalized charge wave functions and have low reorganization energies due to structural rigidity and suppressed torsion relaxation should be targeted for the next generation of OPVs. This approach would mitigate the problem of polaron formation and allow for efficient charge separation with minimal band offsets, greatly increasing the open-circuit voltage and efficiency of OPVs. The superior performance of fullerene-based OPVs is explained by meeting the outlined criteria, as is the performance of recently reported high-efficiency OPVs based on porphyrins (*42*, *43*).

References and Notes

1. R. E. Blankenship, *Molecular Mechanisms of Photosynthesis* (Blackwell Science, Oxford, 2002).
2. T. M. Clarke, J. R. Durrant, *Chem. Rev.* **110**, 6736 (2010).
3. G. Yu, J. Gao, J. C. Hummelen, F. Wudl, A. J. Heeger, *Science* **270**, 1789 (1995).
4. M. M. Wienk *et al.*, *Angew. Chem. Int. Ed.* **42**, 3371 (2003).
5. Y. Kim *et al.*, *Nat. Mater.* **5**, 197 (2006).
6. J. Peet *et al.*, *Nat. Mater.* **6**, 497 (2007).
7. C. R. McNeill *et al.*, *Adv. Funct. Mater.* **18**, 2309 (2008).
8. R.-Q. Png *et al.*, *Nat. Mater.* **9**, 152 (2010).
9. S. H. Park *et al.*, *Nat. Photonics* **3**, 297 (2009).
10. C. Deibel, T. Strobel, V. Dyakonov, *Adv. Mater. (Deerfield Beach Fla.)* **22**, 4097 (2010).
11. S. Shoaee *et al.*, *J. Am. Chem. Soc.* **132**, 12919 (2010).
12. J.-L. Brédas, J. E. Norton, J. Cornil, V. Coropceanu, *Acc. Chem. Res.* **42**, 1691 (2009).
13. T. Strobel, C. Deibel, V. Dyakonov, *Phys. Rev. Lett.* **105**, 266602 (2010).
14. F. Etzold *et al.*, *J. Am. Chem. Soc.* **133**, 9469 (2011).
15. S. Gélinas *et al.*, *J. Phys. Chem. C* **115**, 7114 (2011).
16. A. C. Morteani, P. Sreearunothai, L. M. Herz, R. H. Friend, C. Silva, *Phys. Rev. Lett.* **92**, 247402 (2004).
17. M. R. Jones, *Biochem. Soc. Trans.* **37**, 400 (2009).
18. J. Piris *et al.*, *J. Phys. Chem. C* **113**, 14500 (2009).
19. S. A. Brazovskii, N. N. Kirova, *JETP Lett.* **33**, 4 (1981).
20. D. K. Campbell, A. R. Bishop, K. Fesser, *Phys. Rev. B* **26**, 6862 (1982).
21. X. Wei, Z. V. Vardeny, N. S. Sariciftci, A. J. Heeger, *Phys. Rev. B* **53**, 2187 (1996).
22. R. Österbacka, C. P. An, X. M. Jiang, Z. V. Vardeny, *Science* **287**, 839 (2000).
23. K. Vandewal, K. Tvingstedt, A. Gadisa, O. Inganäs, J. V. Manca, *Nat. Mater.* **8**, 904 (2009).
24. J. G. Müller *et al.*, *Phys. Rev. B* **72**, 195208 (2005).
25. J. G. Müller, U. Lemmer, J. Feldmann, U. Scherf, *Phys. Rev. Lett.* **88**, 147401 (2002).
26. S. V. Frolov, Z. Bao, M. Wohlgenannt, Z. V. Vardeny, *Phys. Rev. B* **65**, 205209 (2002).
27. Materials and methods are available as supporting material on *Science* Online.
28. M. A. Loi *et al.*, *Adv. Funct. Mater.* **17**, 2111 (2007).
29. D. Veldman *et al.*, *J. Am. Chem. Soc.* **130**, 7721 (2008).
30. R. D. Pensack, J. B. Asbury, *J. Am. Chem. Soc.* **131**, 15986 (2009).
31. J. Lee *et al.*, *J. Am. Chem. Soc.* **132**, 11878 (2010).
32. V. I. Arkhipov, P. Heremans, H. Bassler, *Appl. Phys. Lett.* **82**, 4605 (2003).
33. D. Veldman, S. C. J. Meskers, R. A. J. Janssen, *Adv. Funct. Mater.* **19**, 1939 (2009).
34. A. A. Bakulin, D. Martyanov, D. Y. Paraschuk, P. H. M. van Loosdrecht, M. S. Pshenichnikov, *Chem. Phys. Lett.* **482**, 99 (2009).
35. R. A. Marsh, J. M. Hodgkiss, R. H. Friend, *Adv. Mater. (Deerfield Beach Fla.)* **22**, 3672 (2010).
36. J. J. Benson-Smith *et al.*, *Adv. Funct. Mater.* **17**, 451 (2007).
37. K. Vandewal, K. Tvingstedt, A. Gadisa, O. Inganas, J. V. Manca, *Phys. Rev. B* **81**, 125204 (2010).
38. Y. S. Huang *et al.*, *Nat. Mater.* **7**, 483 (2008).
39. J. Holt, S. Singh, T. Drori, Y. Zhang, Z. V. Vardeny, *Phys. Rev. B* **79**, 195210 (2009).
40. T. Drori, J. Holt, Z. V. Vardeny, *Phys. Rev. B* **82**, 075207 (2010).
41. G. D. Scholes, *ACS Nano* **2**, 523 (2008).
42. Y. Matsuo *et al.*, *J. Am. Chem. Soc.* **131**, 16048 (2009).
43. R. F. Service, *Science* **332**, 293 (2011).

Acknowledgments: We thank D. Y. Paraschuk, J. R. Durrant, J. Clark, and T. Strobel for useful discussions. A.A.B. acknowledges a Rubicon Grant from the Netherlands Organization for Scientific Research (NWO), cofinanced by a Marie Curie Cofund Action. A.R. thanks Corpus Christi College for a Research Fellowship. J.C. and D.B. are research fellows of the Belgian National Fund for Scientific Research (FNRS). This project was supported by the Engineering and Physical Sciences Research Council and the RTN SUPERIOR project.

Supporting Online Material

www.sciencemag.org/cgi/content/full/science.1217745/DC1
Materials and Methods
Figs. S1 to S9
Table S1
References (*44*–*49*)

12 December 2011; accepted 10 February 2012
Published online 23 February 2012;
10.1126/science.1217745

Climatic Niche Shifts Are Rare Among Terrestrial Plant Invaders

Blaise Petitpierre,[1] Christoph Kueffer,[2,3] Olivier Broennimann,[1] Christophe Randin,[4] Curtis Daehler,[3] Antoine Guisan[1]*

The assumption that climatic niche requirements of invasive species are conserved between their native and invaded ranges is key to predicting the risk of invasion. However, this assumption has been challenged recently by evidence of niche shifts in some species. Here, we report the first large-scale test of niche conservatism for 50 terrestrial plant invaders between Eurasia, North America, and Australia. We show that when analog climates are compared between regions, fewer than 15% of species have more than 10% of their invaded distribution outside their native climatic niche. These findings reveal that substantial niche shifts are rare in terrestrial plant invaders, providing support for an appropriate use of ecological niche models for the prediction of both biological invasions and responses to climate change.

Niche conservatism in space and time is a key assumption for predicting the impact of global change on biodiversity (*1*, *2*). It is particularly important for the anticipation of biological invasions, which can cause severe damage to biodiversity, economies, and human health (*3*). Niche conservatism implies that species tend to grow and survive under the same environmental conditions in native and invaded ranges (*2*). However, the generality of this assumption is